Langmuir

Article

pubs.acs.org/Langmuir

Wetting Transition on Patterned Surfaces: Transition States and Energy Barriers

Weiqing Ren*

Department of Mathematics, National University of Singapore, Singapore, and Institute of High Performance Computing, Agency for Science, Technology and Research, Singapore

ABSTRACT: We study the wetting transition on microstructured hydrophobic surfaces. We use the string method [*J. Chem. Phys.* **2007**, *126*, 164103; *J. Chem. Phys.* **2013**, *138*, 134105] to accurately compute the transition states, the energy barriers, and the minimum energy paths for the wetting transition from the Cassie−Baxter state to the Wenzel state. Numerical results are obtained for the wetting of a hydrophobic surface textured with a square lattice of pillars. It is found that the wetting of the solid substrate occurs via infiltration of the liquid in a single groove, followed by lateral propagation of the liquid front. The propagation of the liquid front proceeds in a stepwise manner, and a zipping mechanism is observed during the infiltration of each layer. The minimum energy path for the wetting transition goes through a sequence of intermediate metastable states, whose wetted areas reflect the microstructure of the patterned surface. We also study the dependence of the energy barrier on the drop size and the gap between the pillars.

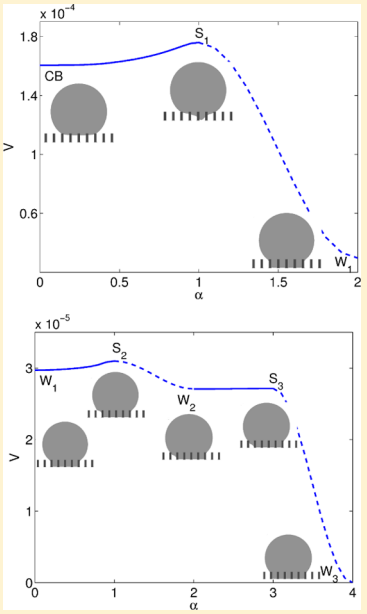

INTRODUCTION

Superhydrophobic surfaces with microscale structures have attracted much attention in both industry and the science community in recent years. This is mainly due to their unique wetting properties and a wide range of applications, e.g., in coating, self-cleaning, and microfluidics.[1] The microstructures on the solid surface can entrap air or vapor pockets, resulting in a composite surface that exhibits superhydrophobic properties. For example, a droplet placed on such a surface has a much larger apparent contact angle compared to that on a smooth surface. This is known as the Cassie−Baxter (CB) state.[2] However, under certain conditions (e.g., thermal fluctuations, external stimuli such as pressure or vibration[3−7]), the liquid can enter the grooves and fully wet the substrate, resulting in the Wenzel (W) state.[8] The transition from the CB state to the W state, called the wetting transition, causes the microstructured surface to lose most of the superhydrophobic features.

Understanding the mechanism of the wetting transition is of primary importance for the design and fabrication of microstructured surfaces. Much effort has been devoted to this problem in recent years, by means of experiments, numerical simulations, and analysis.[4,6,7,9−21] Koishi et al.[9] carried out a "raining" molecular dynamics simulation to compute the probability of a nanodroplet making transition to the wetted state at different impact velocities; the transition probability was then used to find the free energy barrier for the transition. Giacomello et al.[10] used restrained molecular dynamics to compute the free energy along a prescribed reaction coordinate and observed an asymmetric pathway for the wetting transition. In a continuum counterpart of this work,[11] the transition path and the free energy profile were computed using energy minimization along a prescribed reaction coordinate. Recently, Savoy et al. used the forward flux sampling method[12] and boxed molecular dynamics[13] to compute the wetting transition rates and mechanisms for an oily fluid on a surface of nails. Their studies showed that the reentrant geometry can create a free energy barrier for the wetting transition. As in the work of Giacomello et al.,[10,11] a proper choice of an order parameter or reaction coordinate is crucial in these methods. Continuum models were also used to analyze the different wetting regimes and the transition energy barriers.[6,14−18] Conditions for the existence of the Cassie−Baxter and Wenzel states and the transitions between them were derived based the Gibbs free energy. The assumption of a flat fluid−vapor interface may limit the accuracy of these continuum analysis.

Received: November 22, 2013
Revised: January 28, 2014
Published: February 24, 2014

   dx.doi.org/10.1021/la404518q | *Langmuir* 2014, 30, 2879−2885

These earlier work has offered much understanding for the wetting transition. In this paper, we introduce another technique to accurately compute the wetting pathways, the transition states, and the energy barriers.

From the viewpoint of thermodynamics, the CB and W states are minima of the free energy of the system, and the transition from the CB state to the W state is a barrier-crossing event. For the transition to happen, work needs to be done so that the system can overcome the energy barriers separating the two states.[4−7] The transition state theory asserts that saddle points of the energy are the dynamical bottlenecks for the transition, i.e., the transition states.[22−24] Therefore, finding saddle points will reveal the transition mechanism. It also allows one to compute the transition rate.

In this work, we will focus on the overdamped dynamics perturbed by small noise

$$\dot{\phi} = -\nabla V(\phi) + \sqrt{\varepsilon}\xi \tag{1}$$

where $\dot{\phi}$ is the time derivative of ϕ, V is the potential energy, ξ is a white noise, and $\varepsilon \ll 1$. For the dynamics in (1), the transition between the metastable states follows the minimum energy path (MEP).[25−27] The MEP, denoted by φ, is a curve in the configuration space which connects critical points of the energy V and along which the force $-\nabla V$ is parallel to the curve. The MEP satisfies the equation

$$(\nabla V)(\varphi) - (\nabla V, \hat{\tau})\hat{\tau} = 0 \tag{2}$$

where $\hat{\tau}$ is the unit tangent vector to the curve φ. Using the large deviation theory,[28] it can be shown that for the dynamics in (1) and in the zero-temperature limit, the MEP is the most probable transition path, in the sense that the probability that the transition follows any other path is exponentially small.

The purpose of this work is to introduce a numerical technique to accurately compute the saddle points, the energy barriers, and the minimum energy paths for the wetting transition. The main challenge in this problem lies in the complexity of the energy landscape. Because of the small scales in the topography of the solid surface and the pinning of the contact line (the line where the liquid, vapor, and solid intersect) on the microstructures, the energy of the system exhibits many local minima and saddle points, and we expect the transition goes through a sequence of intermediate metastable states. This poses a severe challenge in the computation. Another difficulty arises from the fact that saddle points are unstable critical points of the energy of the system. Traditional optimization methods (e.g., the steepest descent method, the conjugate gradient method, or quasi-Newton method) are inapplicable in the computation of saddle points, and special techniques are required. A number of numerical methods, such as eigenvector following approaches, the dimer method, etc., have been proposed for the identification of saddle points.[29−41] Here we use the climbing string method.[27]

The string method was originally designed for the computation of minimum energy paths between metastable states.[25,26] It was recently extended to the search of saddle points around a given minima.[27] In this work, starting from a local minima (e.g., the CB state), we first use the climbing string method to compute the saddle points that are relevant to the wetting transition and, at the same time, the MEP connecting the minima and the saddle point. Once a saddle point is identified, we let the system relax from the saddle point to the next minima. We repeat this process to compute the transition pathway.

We will illustrate the numerical method using a specific example, in which the solid surface is patterned with a square lattice of rectangular pillars. We will study the problem on the scale of the microstructures. The microstructures are modeled explicitly, and the system is described using a diffuse interface model.

MATHEMATICAL MODEL

The system under study consists of a liquid droplet, which is surrounded by its vapor phase, on a solid substrate. Two immiscible fluids can be treated in the same framework. The solid surface is textured by a square lattice of rectangular pillars (see Figure 1). The pillars have a square lateral cross section

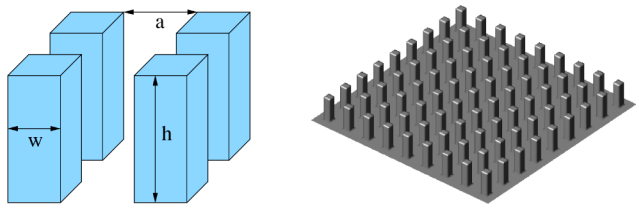

Figure 1. A substrate textured with a square lattice of pillars. The dimensions of the microstructure are the pillar width $w = 0.05$, the gap width $a = 0.12$, and the pillar height h. The pillar and gap widths are fixed in the computation, and the pillar height is varied between 0.12 and 0.18.

with width $w = 0.05$. The height of the pillars ranges from $h = 0.12$ to 0.18 in the simulation. The spacing between pillars is fixed at $a = 0.12$.

The coexistence of the liquid and vapor phases is modeled using the standard diffuse interface model, in which the energy is given by

$$V(\phi) = \int_\Omega \left(\frac{1}{2}\kappa|\nabla\phi|^2 + f(\phi)\right) \mathrm{d}x \tag{3}$$

where ϕ is an order parameter of the fluids, e.g., the density function of the liquid−vapor system. The function $f(\phi)$ is the energy density of the homogeneous phases, and it takes the form of a double-well potential:

$$f(\phi) = \frac{1}{2}\phi^2(\phi - 1)^2 \tag{4}$$

The two minima of f correspond to the two alternative phases: $\phi = 1$ for the liquid phase and $\phi = 0$ for the vapor phase. The thickness of the liquid−vapor interface is determined by κ: $d = \sqrt{\kappa}$. For the numerical results presented in this paper, $\kappa = 10^{-4}$.

At the solid surface, the Dirichlet boundary condition is used for ϕ:

$$\phi = \phi_s \tag{5}$$

Various wettability can be realized by varying ϕ_s in the range $0 \le \phi_s \le 1$ (from nonwetting to wetting).[42] For the numerical results presented below, the value $\phi_s = 0.4$ is used, which yields a static contact angle of 107° on a smooth surface.

Assume the total mass of the fluids is fixed during the wetting transition. Therefore, in the simulation, we impose the constraint

$$\int_\Omega \phi \, \mathrm{d}x = C \tag{6}$$

dx.doi.org/10.1021/la404518q | Langmuir 2014, 30, 2879−2885

where Ω is the region occupied by the fluids and C is the mass of the fluids in the initial CB state.

For the solid surface textured as in Figure 1, the energy functional (3), with the boundary condition (5) and the constraint (6), has many local minima. Two are shown in Figure 2 (top and bottom). The minima on the top is the CB state, in which vapor is trapped under the droplet. The minima on the bottom is a wetted state, in which liquid has entered the grooves on the solid surface. This wetted state is computed using the string method. Details are given in the next section. The apparent contact angle, which is measured by fitting the droplet using a spherical cap, is 141° in the CB state and 133° in the wetted state.

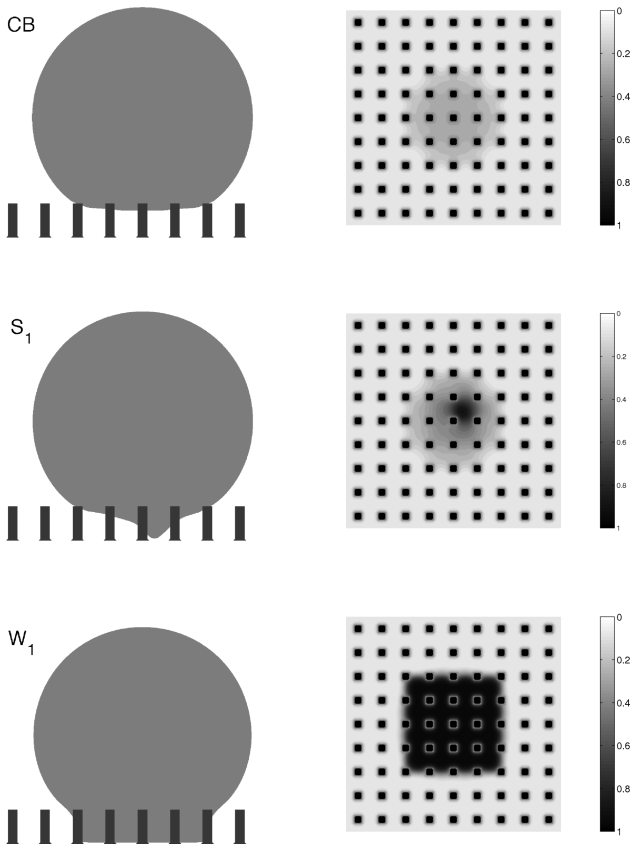

Figure 2. Infiltration of the liquid into the grooves on the substrate. The top panel is the CB state, the middle panel is a transition state (saddle point), and the lower panel is the metastable state (a local minima) that the system goes to after passing the transition state. Figures on the left are the side view of the system, and figures on the right are the top view of the substrate. The gray scale shows the average liquid density within the grooves.

NUMERICAL METHODS

The transition states, energy barriers, and the transition pathway are computed using the string method.[25−27] The overall procedure is as follows. Starting from the CB state, we first use the climbing string method to search for the saddle points around it that are relevant to the wetting transition. In particular, we use the wetted area on the solid surface as a measure of the progress of the wetting transition. Only those saddle points that lead to increasing wetted area are retained. Once such a saddle point is located, we let the system relax from it to find the next minima (an intermediate metastable state). Then we compute the saddle points around the new minima and repeat the above procedure.

The climbing string method finds a saddle point around a given minima a and at the same time the MEP connecting the minima and the saddle point by evolving a string φ in the configuration space. The string is a curve which is parametrized by its normalized arc length α. The string is evolved according to the equation

$$\dot{\varphi}(\alpha, t) = -\frac{\delta V}{\delta \varphi} + \mu + \lambda\hat{\tau}, \quad 0 < \alpha < 1 \tag{7}$$

with the boundary conditions

$$\varphi(\alpha, t) = a, \quad \text{at } \alpha = 0 \tag{8}$$

and

$$\dot{\varphi}(\alpha, t) = -\frac{\delta V}{\delta \varphi} + 2\left(\frac{\delta V}{\delta \varphi}, \hat{\tau}\right)\hat{\tau} + \mu, \quad \text{at } \alpha = 1 \tag{9}$$

where the string ϕ is parametrized by its normalized arc length α, $\dot{\varphi}$ denotes the derivative of ϕ with respect to time t, $\hat{\tau}$ is the unit tangent vector to the string, and $\mu(\alpha)$ and $\lambda(\alpha)$ are the Lagrange multipliers for the mass constraint (6) and the equal arc-length parametrization of the string, respectively. The force $-\delta V/\delta\phi$ associated with the energy (3) is given by

$$-\frac{\delta V}{\delta \varphi} = \kappa\Delta\varphi - f'(\varphi) \tag{10}$$

During the evolution of the string, its initial state at $\alpha = 0$ is fixed at the given minima a. The final state of the string at $\alpha = 1$ is evolved according to the modified force in (9). The force acting on the final state is reversed in the direction tangent to the string. This makes the final state of the string climb uphill on the energy surface in this tangent direction. In the subspace perpendicular to the tangent direction, the system relaxes following the original steepest descent dynamics.

Equations 7−9 are solved with some initial condition $\varphi(\alpha,0) = \varphi_0(\alpha)$ (i.e., the initial string) until a steady state is reached. At the steady state, the final state of the string identifies a saddle point, and the string converges to the MEP connecting the minima a and this saddle point.

In the computation, the string is discretized into $N + 1$ images: $\{\phi_0, \phi_1, ..., \phi_N\}$, where ϕ_0 and ϕ_N are the initial and final states respectively, and $N = 10$ is used for the results reported in the next section. The dynamical equation (7) is solved using a time-splitting scheme:

1. Evolve each image by one time step by solving

$$\dot{\phi}_i = -\frac{\delta V}{\delta \varphi}(\phi_i) + \mu_i, \quad i = 1, 2, ..., N - 1 \tag{11}$$

$$\dot{\phi}_N = -\frac{\delta V}{\delta \varphi}(\phi_N) + 2\left(\frac{\delta V}{\delta \varphi}(\phi_N), \hat{\tau}\right)\hat{\tau} + \mu_N \tag{12}$$

using the Forward Euler method.

2. Redistribute the images along the string according to the equal arc-length parametrization. This is done using polynomial interpolation.

These two steps are repeated until convergence is attained. For details of the numerical algorithm, we refer to the Appendix and the string method.[25−27]

After convergence, the final state ϕ_N locates a saddle point of the energy V. To find the next minima, we perturb this image in

dx.doi.org/10.1021/la404518q | Langmuir 2014, 30, 2879−2885

the direction of the string: $\phi = \phi_N + \varepsilon\hat{\tau}_N$, where $\hat{\tau}_N = (\phi_N - \phi_{N-1})/|\phi_N - \phi_{N-1}|$ and ε is a small parameter, then let it relax according the steepest descent dynamics

$$\dot{\phi} = -\frac{\delta V}{\delta \phi} + \mu \tag{13}$$

At the steady state, ϕ converges to a minima of V, which is an intermediate metastable state in the wetting transition.

RESULTS AND DISCUSSION

The computational domain for each image measures 1.53 × 1.53 × 1.30. The solid surface contains a 9 × 9 array of equally spaced pillars as shown in Figure 1. The images are discretized on a uniform mesh with grid size h = 0.01. The spatial derivatives in the energy (3) and the force (10) are discretized using the centered finite difference.

We first compute the saddle points for the wetting transition out of the CB state. To prepare for the initial string, the CB state is perturbed by a random velocity field that drives the liquid partially into the grooves on the solid surface. This perturbed state serves as the final state of the initial string. The initial string is obtained by the linear interpolation between the CB state and this perturbed state.

Four saddle points are obtained by evolving different initial strings. One is shown in Figure 2 (S_1, the middle panel). The other ones can be obtained by symmetry (rotation of the droplet in the horizontal plane by 90°). From the saddle point configuration, we see that the wetting transition is initiated by a nucleation in a single cavity on the solid surface. Partial infiltration of liquid occurs in this transition state, and the liquid starts to touch the bottom surface. This is consistent with those obtained in molecular dynamics simulation.[12,13] The energy barrier that the system needs to overcome in this inhomogeneous transition is much lower than that in a homogeneous transition (i.e., simultaneous infiltration of liquid into all the grooves under the droplet). Once the system passes the saddle point, it relaxes to a neighboring minima (W_1, the lower panel of Figure 2). In this metastable state, the solid surface under the droplet is fully wetted. The wetted area takes the shape of a square, which reflects the structure of the underlying square lattice. This type of metastable states have been observed in experiments and fluid dynamics simulations.[3]

The energy of the system along the MEP from the CB state to the wetted state W_1 is plotted in Figure 3. The maxima of the energy along the MEP corresponds to the saddle point S_1. The MEP from the CB state to the saddle point is obtained using the climbing string method. The MEP from the saddle point to the wetted state W_1 is computed using the steepest descent dynamics from the saddle point.

Next we apply the same algorithm to compute the transition states and the MEPs for the lateral propagation of the liquid front on the solid surface, starting from the W_1 state. The numerical results are shown in Figure 4. The lateral propagation of the liquid proceeds in a stepwise manner. Figure 4 shows the saddle points and the local minima that the MEP goes through when the liquid front propagates by one layer of the grooves. The propagation starts with a nucleation in the middle of the liquid front. The infiltration of liquid into the new layer occurs from the top of the pillars (the S_2 state). This is followed by propagation of the liquid in opposite directions within the groove (S_2 to W_3). This layer-by-layer propagation

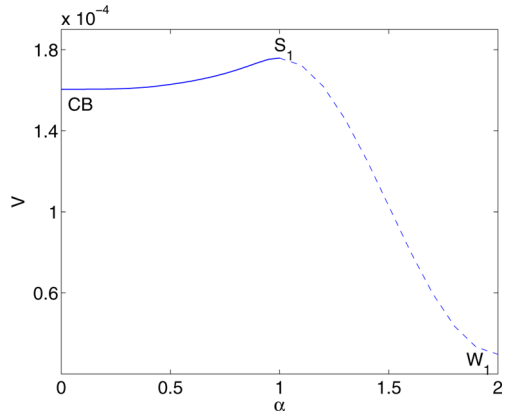

Figure 3. Energy along the MEP from the CB state to the W_1 state shown in Figure 2. The maximum of the energy along the MEP corresponds to the transition state S_1.

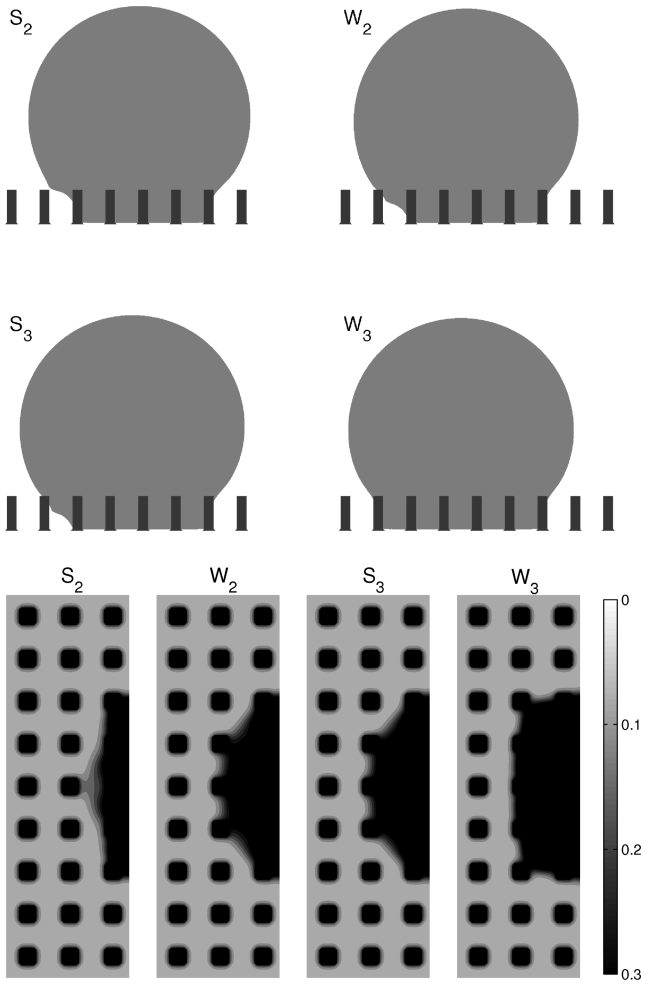

Figure 4. Lateral propagation of the liquid front by one layer of the grooves, from W_1 to W_3. W_2 is an intermediate metastable state (a local minima), S_2 is the transition state (saddle point) from W_1 to W_2, and S_3 is the transition state from W_2 to W_3.

and the zipping mechanism within a layer have been observed before, both in experiments and simulations.[3,13]

The energy along the MEP from W_1 to W_3 is shown in Figure 5. For the geometry and parameters used in this computation, the energy barrier for the lateral propagation at the saddle point S_2 is about 1 order lower than the energy

dx.doi.org/10.1021/la404518q | Langmuir 2014, 30, 2879−2885

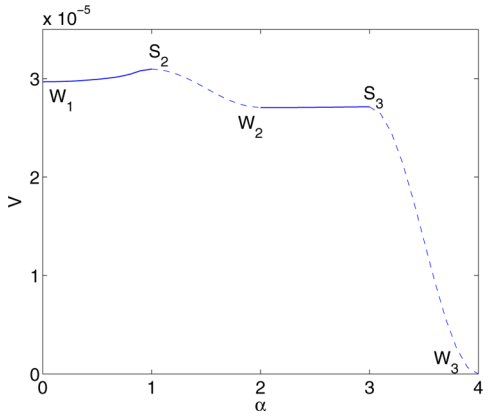

Figure 5. Energy along the MEP from W_1 to W_3 shown in Figure 4.

barrier from the CB state to the W_1 state. This is consistent with those computed using molecular dynamics.[13] We also observe the existence of an intermediate metastable state (W_2) along the MEP. This is caused by the pinning of the contact line at the pillars when the liquid propagates in the groove. For the parameters used in the computation, this barrier is vanishingly small compared to the others.

Finally, we study the dependence of the energy barriers on the pillar height and the drop size. Only the numerical results for the largest barrier at the S_1 state are reported in Figure 6.

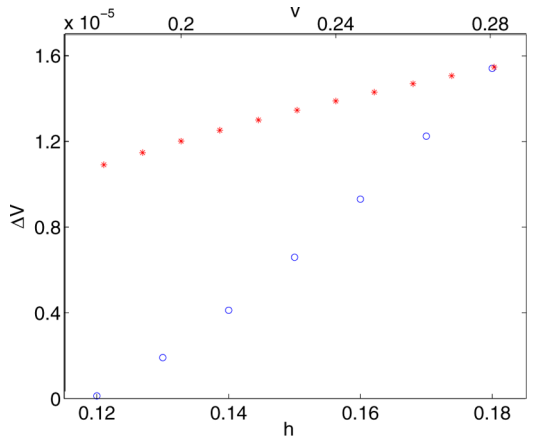

Figure 6. Energy barrier in the CB−W_1 transition at various pillar height (circles) and various drop size (stars). The pillar height is varied from 0.12 to 0.18 (lower axis), and the drop volume relative to the volume of the whole computational domain is varied from 0.18 to 0.28 (upper axis).

The two sets of data are the energy barriers versus the pillar height (lower axis) and the drop size (upper axis), respectively. We see that the energy barrier increases as the pillar height or the drop size increases. The rate of change of the barrier becomes faster at larger pillar height, while the opposite trend is observed for the drop size. Similar trends were observed in molecular dynamics simulations.[13] The energy barrier appears to approach a constant as the drop size is to be further increased.

CONCLUSIONS

In conclusion, we used the string method to study wetting transitions on rough or patterned surfaces. The numerical method allows us to accurately compute the transition states, the energy barriers, and the MEPs for the wetting transition. Using the method, we studied in details the wetting of a hydrophobic surface textured with a square lattice of pillars. Our numerical results revealed the mechanism of the wetting process. Specifically, we observed that the wetting is initiated by infiltration of liquid in a single cavity. This is followed by lateral propagation of the liquid front on the solid surface layer by layer, and rectangle-shaped wetted areas emerge. The filling of each layer also starts locally, from a nucleation in the middle of the liquid front, followed by liquid zipping through the layer. These results are consistent with those observed in experiments or computed using fluid dynamics or molecular dynamics simulations.

The numerical method allows us to study the energy landscape of the liquid−vapor system on a rough surface in a systematic manner. In previous works, this problem has been studied using simplified models in reduced spaces, or simulation of molecular dynamics using prescribed reaction coordinates.

The results are useful for the design and fabrication of microstructured surfaces with certain wetting properties. In this work, we focused on the wetting transition on a surface patterned with a square lattice of rectangular pillars. Nevertheless, the numerical method is general, and it can be applied to solid surfaces with other patterns as well.

The minimum energy paths computed in this work are the most probable transition paths for the steepest descent dynamics (i.e., the constrained Allen−Cahn equation) driven by small noise. In an ongoing work, we are considering a more physical model in which the dynamics is modeled by the stochastic Cahn−Hilliard equation:

$$\frac{\partial \phi}{\partial t} = \nabla\cdot\left(\nabla\frac{\delta V}{\delta \phi} + \sqrt{\varepsilon}\,\xi\right) \tag{14}$$

where ξ is a white noise. Under the Cahn−Hilliard dynamics, the transition still goes through the saddle points, but the pathway will be different. This work will be presented in a subsequent paper.

APPENDIX: SIMULATION DETAILS

In the simulation, the string is discretized into $N + 1$ images. At each time step, these images are first evolved by the forward Euler method and then redistributed along the string according to equal arc length using a polynomial interpolation.

Let Δt be the time step in the Euler method. Denote by ϕ_i^k, $i = 0, ..., N$, the position of the images after k iterations and f_i^k the potential force on the image ϕ_i^k, i.e., $f_i^k = -(\delta V/\delta\varphi)(\phi_i^k)$. Then the new set of images after the first step is given by

$$\phi_i^* = \phi_i^k + \Delta t\mathcal{P}(f_i^k), \quad i = 1, ..., N-1 \tag{15}$$

$$\phi_N^* = \phi_N^k + \Delta t\mathcal{P}(f_N^k - 2(f_N^k, \hat{\tau}^k)\hat{\tau}^k) \tag{16}$$

where $\mathcal{P}(f)$ is the projection of f to the manifold on which the mean of f equals zero:

$$\mathcal{P}(f) = f(x) - \frac{1}{|\Omega|}\int_\Omega f\,dx \tag{17}$$

The purpose of the projection is to impose the constant volume constraint on the droplet.

In the second step, the intermediate images ϕ_i^*, $i = 1, ..., N-1$, are redistributed along the string using the cubic polynomial

dx.doi.org/10.1021/la404518q | Langmuir 2014, 30, 2879−2885

interpolation. This is done as follows. We first compute the arc length corresponding to the images ϕ_i^*

$$s_0 = 0, \quad s_i = s_{i-1} + |\phi_i^* - \phi_{i-1}^*|, \quad i = 1, ..., N \tag{18}$$

The normalized arc length is then obtained by $\alpha_i^* = s_i/s_N$. Next we interpolate the data points $\{(\alpha_i^*,\phi_i^*), i = 0, ..., N\}$ using cubic polynomials to obtain the new images ϕ_i^{k+1} on the uniform mesh $\alpha_i = i/N$. Because of numerical errors in the interpolation, the new images will be off the constant volume manifold. Therefore, another projection is carried out to enforce the constant volume constraint.

The above two steps are repeated until a steady state is reached. At the steady state, the final point ϕ_N identifies a saddle point, and the string converges to the MEP connecting the minima at ϕ_0 and the saddle point.

AUTHOR INFORMATION

Corresponding Author

*E-mail: matrw@nus.edu.sg.

Notes

The authors declare no competing financial interest.

ACKNOWLEDGMENTS

The author is grateful to Weinan E for stimulating discussions. The work was supported in part by Singapore A*STAR SERC PSF grant R-146-000-173-305 (Project No. 1321202071) and A*STAR SERC "Complex Systems Programme" R-146-000-171-305 (Project No. 1224504056).

REFERENCES

(1) de Gennes, P. G.; Brochard-Wyart, F.; Quéré, D. *Capillarity and Wetting Phenomena: Drops, Bubbles, Pearls, Waves*; Springer: New York, 2003.

(2) Cassie, A. B. D.; Baxter, S. Wettability of porous surfaces. *Trans. Faraday Soc.* **1944**, *40*, 546.

(3) Sbragaglia, M.; Peters, A. M.; Pirat, C.; Borkent, B. M.; Lammertink, R. G. H.; Wessling, M.; Lohse, D. Spontaneous breakdown of superhydrophobicity. *Phys. Rev. Lett.* **2007**, *99*, 156001.

(4) Bormashenko, E.; Pogreb, R.; Whyman, G.; Bormashenko, Y.; Erlich, M. Vibration-induced Cassie-Wenzel wetting transition on rough surfaces. *Appl. Phys. Lett.* **2007**, *90*, 201917.

(5) Yoshimitsu, Z.; Nakajima, A.; Watanabe, T.; Hashimoto, K. Effects of surface structure on the hydrophobicity and sliding behavior of water droplets. *Langmuir* **2002**, *18*, 5818−5822.

(6) He, B.; Patankar, N. A.; Lee, J. Multiple equilibrium droplets shapes and design criterion for rough hydrophobic surfaces. *Langmuir* **2003**, *19*, 4999.

(7) Bico, J.; Marzolin, C.; Quéré, D. Pearl drops. *Europhys. Lett.* **1999**, *47*, 220.

(8) Wenzel, R. N. Resistance of solid surfaces to wetting by water. *Ind. Eng. Chem.* **1936**, *28*, 988−994.

(9) Koishi, T.; Yasuoka, K.; Fujikawa, S.; Ebisuzaki, T.; Zeng, X. C. Coexistence and transition between Cassie and Wenzel state on pillared hydrophobic surface. *Proc. Natl. Acad. Sci. U. S. A.* **2009**, *106*, 8435.

(10) Giacomello, A.; Meloni, S.; Chinappi, M.; Casciola, C. M. Cassie-Baxter and Wenzel states on a nanostructured surface: Phase diagram, metastabilities, and transition mechanism by atomistic free energy calculations. *Langmuir* **2012**, *28*, 10764−10772.

(11) Giacomello, A.; Chinappi, M.; Meloni, S.; Casciola, C. M. Metastable wetting on superhydrophobic surfaces: Continuum and atomistic views of the Cassie-Wenzel transition. *Phys. Rev. Lett.* **2012**, *109*, 226102.

(12) Savoy, E. S.; Escobedo, F. A. Molecular simulations of wetting of a rough surface by an oily fluid: Effect of topology, chemistry, and droplet size on wetting transition rates. *Langmuir* **2012**, *28*, 3412−3419.

(13) Savoy, E. S.; Escobedo, F. A. Simulation study of free-energy barriers in the wetting transition of an oily fluid on a rough surface with reentrant geometry. *Langmuir* **2012**, *28*, 16080−16090.

(14) Marmur, A. Wetting on hydrophobic rough surfaces: To be heterogeneous or not to be? *Langmuir* **2003**, *19*, 8343.

(15) Marmur, A. The lotus effect: Super-hydrophobicity and metastability. *Langmuir* **2004**, *20*, 3517−3519.

(16) Patankar, N. A. On the modeling of hydrophobic contact angles on rough surfaces. *Langmuir* **2003**, *19*, 1249.

(17) Patankar, N. A. Transition between superhydrophobic states on rough surfaces. *Langmuir* **2004**, *20*, 7097−7102.

(18) Patankar, N. A. Consolidation of hydrophobic transition criteria by using an approximate energy minimization approach. *Langmuir* **2010**, *26*, 8941−8945.

(19) Ishino, C.; Okumura, K.; Quéré, D. Wetting transitions on rough surfaces. *Europhys. Lett.* **2004**, *68*, 419−425.

(20) Ishino, C.; Okumura, K. Nucleation scenario for wetting transition on textured surfaces: The effect of contact angle hysteresis. *Europhys. Lett.* **2006**, *76*, 464−470.

(21) Peters, A. M.; Pirat, C.; Sbragaglia, M.; Borkent, B. M.; Wessling, M.; Lohse, D.; Lammertink, R. G. H. Cassie-Baxter to Wenzel state wetting transition: Scaling of the front velocity. *Eur. Phys. J. E* **2009**, *29*, 391.

(22) Eyring, H. The activated complex in chemical reactions. *J. Chem. Phys.* **1935**, *3*, 107.

(23) Wigner, E. The transition state method. *Trans. Faraday Soc.* **1938**, *34*, 29−41.

(24) Horiuti, J. On the statistical mechanical treatment of the absolute rate of the chemical reaction. *Bull. Chem. Soc. Jpn.* **1938**, *13*, 210.

(25) E, W.; Ren, W.; Vanden-Eijnden, E. String method for the study of rare events. *Phys. Rev. B* **2002**, *66*, 052301.

(26) E, W.; Ren, W.; Vanden-Eijnden, E. Simplified and improved string method for computing the minimum energy paths in barrier-crossing events. *J. Chem. Phys.* **2007**, *126*, 164103.

(27) Ren, W.; Vanden-Eijnden, E. A climbing string method for saddle point search. *J. Chem. Phys.* **2013**, *138*, 134105.

(28) Freidlin, M. I.; Wentzell, A. D. *Random Perturbations of Dynamical Systems*, 2nd ed.; Springer: New York, 1998.

(29) Crippen, G. M.; Scheraga, H. A. Minimization of polypeptide energy: Xi. the method of gentlest ascent. *Arch. Biochem. Biophys.* **1971**, *144*, 462.

(30) Cerjan, C. J.; Miller, W. H. On finding transition states. *J. Chem. Phys.* **1981**, *75*, 2800.

(31) Simons, J.; Jorgensen, P.; Taylor, H.; Ozment, J. Walking on potential energy surfaces. *J. Phys. Chem.* **1983**, *87*, 2745.

(32) Bell, S.; Crighton, J. S. Locating transition states. *J. Chem. Phys.* **1984**, *80*, 2464.

(33) Banerjee, A.; Adams, N.; Simons, J.; Shepard, R. Search for stationary points on surfaces. *J. Phys. Chem.* **1985**, *89*, 52.

(34) Baker, J. An algorithm for the location of transition states. *J. Comput. Chem.* **1986**, *7*, 385.

(35) Ayala, P. Y.; Schlegel, H. B. A combined method for determining reaction paths, minima, and transition state geometries. *J. Chem. Phys.* **1997**, *107*, 375.

(36) Munro, L. J.; Wales, D. J. Defect migration in crystalline silicon. *Phys. Rev. B* **1999**, *59*, 3969.

(37) Kumeda, Y.; Wales, D. J.; Munro, L. J. Transition states and rearrangement mechanisms from hybrid eigenvector-following and density functional theory: Application to $C_{10}H_{10}$ and defect migration in crystalline silicon. *Chem. Phys. Lett.* **2001**, *185*, 341.

(38) Mousseau, N.; Barkema, G. T. Traveling through potential energy landscapes of disordered materials: The activation-relaxation technique. *Phys. Rev. E* **1998**, *57*, 2419.

(39) Henkelman, G.; Jónsson, H. A dimer method for finding saddle points on high dimensional potential surfaces using only first derivatives. *J. Chem. Phys.* **1999**, *111*, 7010.

(40) E, W.; Zhou, X. The gentlest ascent dynamics. *Nonlinearity* **2011**, *24*, 1831.
(41) Zhang, J.; Du, Q. Shrinking dimer dynamics and its applications to saddle points search. *SIAM J. Numer. Anal.* **2012**, *50*, 1899.
(42) Borcia, R.; Borcia, I. D.; Bestehorn, M. Drops on an arbitrarily wetting substrate: A phase field description. *Phys. Rev. E* **2008**, *78*, 066307.

dx.doi.org/10.1021/la404518q | *Langmuir* 2014, 30, 2879−2885